

Universal intrinsic higher-rank spin Hall effect

Junpeng Hou¹ and Chuanwei Zhang¹

¹*Department of Physics, The University of Texas at Dallas, Richardson, Texas 75080-3021, USA*

Spin Hall effect (SHE), a fundamental transport phenomenon with non-zero spin current but vanishing charge current, has important applications in spintronics for the electrical control of spins. Owing to the half-spin nature of electrons, the rank of spin current (determined by the rank of spin tensor) has been restricted to 0 and 1 for charge and spin Hall effects. Motivated by recent studies of pseudospin-1 fermions in solid state and cold atomic systems, here we introduce and characterize higher-rank (≥ 2) SHEs in large spin (≥ 1) systems. We find a universal rank-2 spin Hall conductivity $e/4\pi$ (with zero rank-0 and 1 conductivities) for a spin-1 model with intrinsic spin-orbit (SO) coupling. Similar rank-2 SHEs can also be found in a spin-3/2 system. An experimental scheme is proposed to realize the required SO coupling for rank-2 SHEs with pseudospin-1 fermionic atoms in an optical lattice. Our results reveal novel spin transport phenomena in large spin systems and may find important applications in designing innovative spintronic devices.

Introduction. Hall effects and their quantized siblings are one of the major cornerstones of modern condensed-matter physics, and the discovery of novel Hall effects often opens new avenues for controlling electronic transport for device applications. The most notable example in this context is probably the spin Hall effect (SHE), where spin up and down of electrons move along opposite transverse directions under an applied electric field, yielding non-zero spin current but vanishing charge current (see Fig. 1(a) for an illustration) [1, 2]. Spin-current-based phenomena such as giant SHE [3–5], inverse SHE [6–10] and quantum SHE [11–13], have also been widely studied. SHE provides a powerful tool for controlling spins electrically, thus has significant applications for realizing low-power spintronic devices [2].

The origin of SHE can be attributed to either extrinsic impurity scattering [14] or intrinsic spin-orbit (SO) coupling [15, 16]. In intrinsic SHE, the SO coupling serves as an effective magnetic field that is opposite for spin up and down, yielding nonzero spin-Hall current. For instance, in a two-dimensional (2D) electronic gas, the Rashba SO coupling yields a spin-Hall conductivity $e/8\pi$, which is a universal constant that does not depend on the underlying material properties [16]. Here the spin current operator is generally defined by $\frac{\hbar}{4}\{\sigma_z, \hat{v}\}$ through the rank-1 Pauli matrix σ_z , where $\{\cdot, \cdot\}$ denotes the anticommutator and \hat{v} is the velocity operator. In this sense, the charge-current operator $\sigma_0 \hat{v}$ can be taken as rank-0. For electrons with half spins, 0 and 1 are only available ranks for spin-1/2 matrices.

Recent theoretical and experimental advances in the study of pseudospin-1 fermions have opened a new perspective towards the realization of novel quantum phases and dynamics in large-spin systems, in which higher-rank spin-tensors exist and play a crucial role [17]. In particular, triply-degenerate fermions were proposed as novel quasiparticles without counterparts in quantum field theory [18, 19] and certain experimental signatures have been observed in solid-state materials [20]. Moreover, large-spin ($> 1/2$) is easily accessible in experiments for

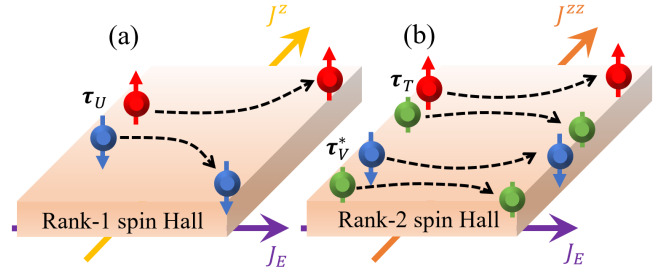


FIG. 1: Illustration of higher-rank spin-Hall effect. (a) In rank-1 SHE, the red (spin up) and blue (spin down) components move along opposite directions, yielding a vanishing rank-0 charge Hall current but a finite rank-1 spin Hall current \mathbf{J}_1^z . (b) Rank-2 SHE in a spin-1 fermionic system, where both charge (rank-0) and rank-1 spin currents vanish, leaving only non-zero rank-2 spin current \mathbf{J}_2^{zz} . The red, green and blue disks correspond to spin components $|m_z = 1\rangle$, $|0\rangle$ and $|-1\rangle$ respectively. In both cases, the electric field is applied along the x direction, leading to a charge current \mathbf{J}_E while transverse charge current \mathbf{J}_0 remains zero.

ultracold atoms with multiple hyperfine states [21–23], which can host interesting quantum phases [24–28] and topological states [29–32].

While these works reveal many fascinating phenomena, spin transport in large spin systems, particularly when involving higher-rank spin tensors, remains largely unexplored. A natural question is whether there is intrinsic higher-rank (≥ 2) SHE where the lower-rank spin and charge currents are zero. Here the rank of the spin current is defined through the spin matrix rank in the spin current operator. If so, can the higher-rank spin-Hall conductivity be a universal constant independent of material properties? Can we realize and observe higher-rank SHE in a realistic physical system?

In this Letter, we address these important questions by defining and characterizing *universal intrinsic higher-rank SHE* and exploring its experimental realization. Our main results are:

- i) Utilizing Cartan subalgebra of $SU(N)$ group, we de-

fine spin currents of different ranks in large spin systems and introduce the concept of higher-rank SHE.

ii) We develop a minimum spin-1 model for realizing rank-2 SHE with intrinsic 2D spin-tensor-momentum (STM) coupling. We find that the rank-2 spin-Hall conductivity is a universal constant $e/4\pi$, independent of material properties, and rank-0 charge-Hall and rank-1 spin-Hall conductivities are zero. This is confirmed by solving both spin dynamics and linear response theory. We further showcase another rank-2 SHE in a spin-3/2 model.

iii) We propose an experimental scheme for realizing the 2D STM coupling in the minimal spin-1 model of rank-2 SHE. This is done by utilizing ultracold fermions in a 2D STM-coupled optical lattice, which is built upon recent experimental advances on realizations of 2D SO coupling for pseudospin-1/2 atoms [33].

Higher-rank spin currents and spin-Hall effect. Mathematically, it is well-known that a spin- F Hamiltonian can be expanded using the generators of the $SU(N)$ ($N = 2F + 1$) group. Those generators are traceless and symmetric, and can be constructed as rank- n ($n \leq r_s$) spin tensors from spin vectors $F_i, i = x, y, z$. Here $r_s = N - 1$ is the rank of $SU(N)$ group. For instance, there are up to rank-2 spin tensors defined as $N_{ij} = \{F_i, F_j\}/2 - \delta_{ij}F^2/3$ in a spin-1 system [17].

We use a Cartan subalgebra $\{F_z, N_{zz}, \dots, N_{zz\dots z}\}$ of $SU(N)$ to define rank- n spin polarization $P_n = \frac{\hbar}{2}N_{zz\dots z}$ (with n subscripts) and spin current density $\mathbf{J}_n^{zz\dots z} = \frac{1}{2}\{P_n, \hat{\mathbf{v}}\}$ operators. For $n = 1$, the definition naturally yields usual rank-1 spin polarization $\langle F_z \rangle = \frac{\hbar}{2}\psi^\dagger F_z \psi$ and spin current density $\langle \mathbf{J}_1^z \rangle = \frac{1}{2}\text{Re}\psi^\dagger \{F_z, \hat{\mathbf{v}}\} \psi$, where ψ is the spinor state of the particle. Note that the charge current $\langle \mathbf{J}_0 \rangle = \text{Re}\psi^\dagger \hat{\mathbf{v}} \psi$ can be treated as the current of rank-0 unit matrix I .

For widely studied intrinsic universal rank-1 SHE in spin-1/2 electrons, the applied electric field induces non-zero transverse spin current, but zero charge current, as illustrated in Fig. 1(a). Similarly, we can define rank- n SHE as that with only non-zero rank- n spin current (spin currents with different ranks, including charge current, all vanish). Clearly, the first example is the rank-2 SHE, which requires at least a spin-1 system. The corresponding spin current configuration is illustrated in Fig. 1(b), where both spin $|1\rangle$ and $|-1\rangle$ moves in the same direction for vanishing rank-1 spin current, while a doubled spin $|0\rangle$ current flows in the opposite direction for the sake of zero charge current. Since the Cartan subalgebra is complete up to a constant, this configuration implies that there must be a non-vanishing rank-2 spin current. Such a completeness also guarantees that a rank- n SHE can always be defined.

Universal intrinsic rank-2 spin-Hall effect. A general form of SO coupling in a spin-1 system may lead to non-zero spin currents with different ranks. In order to find suitable SO coupling for rank-2 SHE, we adopt the Gell-

Mann matrix representation $\lambda_i, 1 \leq i \leq 8$ for the $SU(3)$ group, which can be grouped into three different $SU(2)$ subalgebras [34]

$$\boldsymbol{\tau}_T = \{\lambda_1, \lambda_2, \lambda_3\}, \boldsymbol{\tau}_U = \{\lambda_4, \lambda_5, \lambda_+\}, \boldsymbol{\tau}_V = \{\lambda_6, \lambda_7, \lambda_-\}. \quad (1)$$

in the spin subspaces $\{|+1\rangle, |0\rangle\}_T, \{|+1\rangle, |-1\rangle\}_U$ and $\{|0\rangle, |-1\rangle\}_V$. Here $\lambda_\pm = \frac{\sqrt{3}}{2}\lambda_8 \pm \frac{1}{2}\lambda_3$ and $\lambda_+ = F_z/2$. Physically, each subalgebra spans the symmetry group of a quantum half spin.

For each $SU(2)$ subalgebra, we consider the intrinsic SHE with Rashba SO coupling [16]

$$H_i^{\text{Rashba}} = \frac{p^2}{2m} - \frac{\lambda}{\hbar} \boldsymbol{\tau}_i \cdot (\hat{\mathbf{z}} \times \mathbf{p}), \quad (2)$$

where m is the effective mass of electron, $\lambda > 0$ is the Rashba coupling strength and $\hat{\mathbf{z}}$ is the unit vector along the z direction. When the electric field E_x is applied along the x direction (Fig. 1), there is a rank-1 spin Hall conductivity $\sigma_{xy} = \frac{e}{8\pi}$ [16]. The Hall conductivity can be computed using the Kubo formula

$$\sigma_{xy} = \frac{e\hbar}{V} \sum_{\mathbf{k}, n \neq n'} (f_{n'\mathbf{k}} - f_{n\mathbf{k}}) \frac{\text{Im} \langle n'\mathbf{k} | J_{n,x} | n\mathbf{k} \rangle \langle n\mathbf{k} | v_y | n'\mathbf{k} \rangle}{(E_{n\mathbf{k}} - E_{n'\mathbf{k}})^2}, \quad (3)$$

where V is unit cell volume, n, n' are band indices, $f_{n\mathbf{k}}$ is the Fermi-Dirac distribution, the velocity operator $\hat{\mathbf{v}} = \partial_{\mathbf{p}} H$, \mathbf{J}_n is the Hall-current operator. $E_{n\mathbf{k}}$ and $|n\mathbf{k}\rangle$ are eigenvalues and eigenvectors in momentum space. The corresponding rank-1 spin current operator is defined as $\mathbf{J}_1^z = \frac{1}{2} \{ \frac{\hbar}{2} \tau_{i,z}, \hat{\mathbf{v}} \}$.

The three $SU(2)$ subalgebras are not independent and there are only $r_s = 2$ diagonal generators for Cartan subalgebra (here $[\lambda_3, \lambda_8] = 0$). Through blending two of the subalgebras, we construct the following Hamiltonian

$$H_{F=1} = \frac{p^2}{2m} - \frac{1}{\sqrt{2}} \frac{\lambda}{\hbar} (\boldsymbol{\tau}_T + \boldsymbol{\tau}_V^*) \cdot (\hat{\mathbf{z}} \times \mathbf{p}), \quad (4)$$

where $(\boldsymbol{\tau}_T + \boldsymbol{\tau}_V^*) \cdot (\hat{\mathbf{z}} \times \mathbf{p}) = -ip \begin{pmatrix} 0 & e^{-i\theta_{\mathbf{p}}} & 0 \\ e^{i\theta_{\mathbf{p}}} & 0 & e^{i\theta_{\mathbf{p}}} \\ 0 & e^{-i\theta_{\mathbf{p}}} & 0 \end{pmatrix}$

describes a 2D STM coupling. The resulting band structure is plotted in Fig. 2(a), which exhibits a 2D triply-degenerate point at $\mathbf{p} = 0$. When the Fermi level lays above the triply-degenerate point, the Fermi surfaces are simply concentric circles due to isotropic SO coupling, as shown in Fig. 2(a).

Applying the Kubo formula with the rank-2 spin current operator $\mathbf{J}_2^{zz} = \frac{1}{2} \{ \frac{\hbar}{2} N_{zz}, \mathbf{v} \}$, we find a non-vanishing rank-2 spin-Hall conductivity

$$\sigma_{xy}^{zz} = \frac{e}{4\pi}, \quad (5)$$

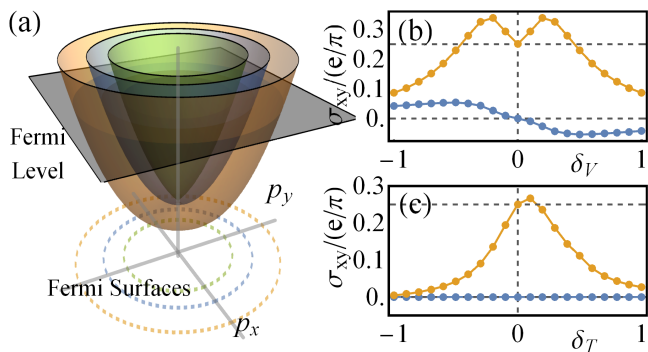


FIG. 2: (a) Representative energy spectrum of the Hamiltonian in Eq. 4. (b) and (c) Rank-1 (blue) and rank-2 (orange) spin-Hall conductivities with respect to vector and tensor Zeeman fields δ_V and δ_T . $E_F = 1$ and $p_F = 1$ are taken as units for energy and momentum. The corresponding dimensionless parameters are set as $m = 0.2$ and $\lambda = 0.5$.

while charge and rank-1 spin Hall conductivities $\sigma_{xy}^c = \sigma_{xy}^z = 0$. We note that $\sigma_{xy}^{zz} = \frac{e}{4\pi}$ is a universal constant that is independent of the material parameters such as SO coupling strength or effective mass. Therefore the model Hamiltonian Eq. 4 describes a simple yet nontrivial system exhibiting universal higher-rank SHE.

To understand the physical mechanism of this rank-2 SHE, we notice that $\boldsymbol{\tau}_T \cdot (\hat{\mathbf{z}} \times \mathbf{p})$ yields rank-1 SHE where $|+1\rangle$ and $|0\rangle$ spin components move in opposite transverse directions, rendering a rank-1 spin-Hall conductivity $\sigma_{xy}^T = \frac{e}{8\pi}$ (see Fig. 1(b)). Accordingly, the conjugate term $\boldsymbol{\tau}_T^* \cdot (\hat{\mathbf{z}} \times \mathbf{p})$ leads to opposite spin flow, yielding a negative $\sigma_{xy}^{T*} = -\frac{e}{8\pi}$. While this can be verified by the Kubo formula, a more insightful way is to look at the Bloch equation [16]

$$\hbar \frac{d\mathbf{n}}{dt} = \mathbf{n} \times \boldsymbol{\Delta} + \eta_d \hbar \frac{d\mathbf{n}}{dt} \times \mathbf{n}, \quad (6)$$

where \mathbf{n} is the direction of the doublet, $\boldsymbol{\Delta}$ is the Zeeman coupling (i.e. the SO coupling term) and η_d is some small damping effects. The above equation can be solved using Green function techniques. Considering the region where linear response theory applies and keeping only leading-order terms, we have

$$n_z = -\frac{e\hbar^2 E_x p_y}{2\lambda p^3}, \quad (7)$$

whose sign can be reversed by changing that of p_y . Notice that

$$\boldsymbol{\tau}_T^* \cdot (\hat{\mathbf{z}} \times \mathbf{p}) = \boldsymbol{\tau}_T \cdot (\hat{\mathbf{z}} \times (\mathcal{I}\mathbf{p}\mathcal{I}^{-1})), \quad (8)$$

where \mathcal{I} denotes spatial inversion along \hat{y} . Therefore n_z gains an opposite sign between Rashba SO coupling and its conjugate term, leading to opposite rank-1 spin Hall conductivities. Similar argument also applies to other subalgebras $\boldsymbol{\tau}_U$ and $\boldsymbol{\tau}_V$.

From above argument, $\boldsymbol{\tau}_V^*$ conjugate Rashba SO coupling dictates the $|0\rangle/|-1\rangle$ components flow along the same direction as the $|0\rangle/|+1\rangle$ components under $\boldsymbol{\tau}_T$, which give the rank-2 SHE illustrated in Fig. 1(b). The rank-2 spin-Hall conductivity is doubled $\sigma_{xy}^{zz} = 2\sigma_{xy}^T$ due to the fact that each channel (n, n') is enhanced by a factor 2 while only channels $(+, -)/(-, +)$ contributes to σ_{xy}^{zz} .

Besides the rank-2 spin current \mathbf{J}_2^{zz} , we can similarly define other higher-rank currents like \mathbf{J}_2^{xy} or \mathbf{J}_2^{yz} , and the corresponding Hall conductivities usually vanish in the above model. However, we notice the following constraint

$$\sigma_{xy}^{xx} + \sigma_{xy}^{yy} + \sigma_{xy}^{zz} = 0 \quad (9)$$

holds as long as the charge current is zero. This constraint can be easily proved since \mathbf{F}^2 must be a multiple of unit matrix by Schur's lemma (i.e., the total spin is conserved). Applying the Kubo formula, we find

$$\sigma_{xy}^{xx} = 0 \text{ and } \sigma_{xy}^{yy} = -\frac{e}{4\pi}, \quad (10)$$

which indeed satisfy the above constraint.

When the spin term in Eq. 4 changes to $\boldsymbol{\tau}_T + \boldsymbol{\tau}_V$ (i.e., a spin vector), there is only rank-1 SHE based on above argument, where the current of spin component $|0\rangle$ is cancelled out. Apply the Kubo formula, we find $\sigma_{xy}^z = \frac{e}{2\pi}$ because the contribution counts both $(\pm, 0)$ and $(0, \pm)$. Moreover, all rank-2 spin Hall conductivities vanish so that Eq. 9 is trivially satisfied. Since $F_y = \sqrt{2}(\lambda_2 + \lambda_7)$ and $F_x = \sqrt{2}(\lambda_1 + \lambda_6)$, this model is a direct generalization of Rashba SO coupling to a spin-1 system [30].

Effect of Zeeman fields. Generally, for a spin-1 system discussed above, the Zeeman fields contain both spin-vector and spin-tensor terms as $\frac{\delta_V \hbar}{2} F_z + \frac{\delta_T \hbar}{2} F_z^2$. Both fields lift the triply-degenerate point at $\mathbf{p} = 0$ and spoil the universality of the spin Hall conductivity. We numerically compute the spin-Hall conductivities under a given Fermi energy, which are shown in Figs. 2(b) and (c) for both δ_V and δ_T .

Changing the sign of δ_V is equivalent to a \mathbb{Z}_2 rotation between spin components $|1\rangle$ and $|-1\rangle$, under which spin-tensor polarization $\frac{\hbar}{2}\langle N_{zz} \rangle$ is unchanged while spin-vector polarization $\frac{\hbar}{2}\langle F_z \rangle$ gains a minus sign, indicating symmetric and antisymmetric responses from σ_{xy}^{zz} and σ_{xy}^z shown in Fig. 2(b). When $|\delta_V|$ increases, both $|\sigma_{xy}^z|$ and $|\sigma_{xy}^{zz}|$ increase to their maxima and then decrease. σ_{xy}^{zz} drops more rapidly as the top band shifts away from the Fermi level. When $\delta_V \rightarrow \pm\infty$, both conductivities approach 0 since the system becomes a flat-band insulator.

The tensor Zeeman field $\delta_T F_z^2/2$ has the same effect on $|1\rangle$ and $|-1\rangle$, therefore σ_{xy}^{zz} is asymmetric while σ_{xy}^z remains zero (see Fig. 2(c)). There would also be small non-zero charge-current conductance, which is not plotted in the panel. When $\delta_T > 0$, it shifts both top and

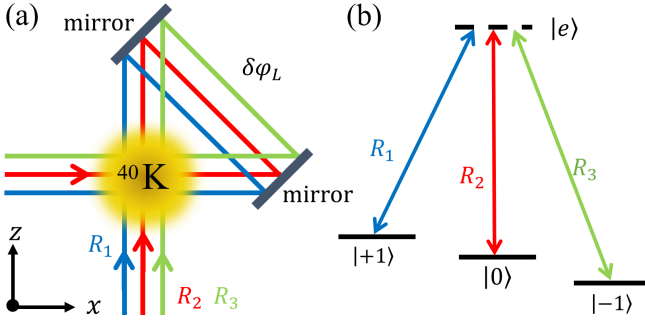


FIG. 3: Illustration of the experimental scheme for realizing STM coupling for the rank-2 SHE in Eq. 4. (a) Laser setup consisting of three Raman lasers R_1 (Blue, plane-wave), R_2 (red, standing wave) and R_3 (green, plane wave). φ_L denotes the phase accumulated by lasers in the triangle optical path K formed by the atomic gas and two mirrors. Then $\delta\varphi_L$ is the differences between the accumulated phase. (b) The coupling between three spin states under the Raman lasers with proper frequencies.

bottom bands upward and they become nearly degenerate under extremely large Zeeman field. The rank-2 spin-Hall conductance σ_{xy}^{zz} first rises and then gradually approaches 0. When $\delta_T < 0$, all three bands remain intersecting the Fermi level and σ_{xy}^{zz} monotonically decreases.

Generalization to larger spin. A rank-2 SHE can also be realized in a spin-3/2 system. Consider a 2D spin-3/2 Hamiltonian

$$H_{F=\frac{3}{2}} = \frac{p^2}{2m} - \frac{\lambda}{\hbar}(\tau_{1,2} + \tau_{3,4}^*) \cdot (\hat{z} \times \mathbf{p}), \quad (11)$$

where $\tau_{1,2}$ and $\tau_{3,4}$ represent SU(2) subalgebra for $|m_z > 0\rangle$ and $|m_z < 0\rangle$ respectively [38]. The Hamiltonian is block-diagonalized since the spin components $|m_z > 0\rangle$ or $|m_z < 0\rangle$ are coupled separately. The Hamiltonian describes two decoupled rank-1 SHEs defined by $\tau_{1,2,z}$ and $\tau_{3,4,z}$ in two subspaces. Specifically, spin components $|m_z\rangle$ and $| -m_z\rangle$ flow along the same direction, which is opposite to that of $|m_z \pm 2\rangle$ (– for $m_z > 0$ and + for $m_z < 0$). Consequently, there is only non-vanishing rank-2 spin current with Hall conductivity $\sigma_{xy}^{zz} = \frac{e}{\pi}$.

For a general SU(N) group, we can use the generalized Gell-Mann matrices [35], from which the SU(2) subalgebras could be defined. Hamiltonians for realizing different ranks of SHEs may be constructed using the SO coupling based on such SU(2) subgroups.

Potential experimental realization. Recently, 2D SO coupling for spin-1/2 systems has been experimentally realized in cold atoms [33, 36, 37]. Here we propose that similar experimental setup [33] can also be used to realize the STM coupling in the model Hamiltonian Eq. 4 using a pseudospin-1 ultracold atomic gas.

We use three hyperfine states of atoms to define (pseudo)spin states $|+1\rangle$, $|0\rangle$, and $|-1\rangle$. As demonstrated in Ref. [33], either $\tau_T \cdot (\hat{z} \times \mathbf{p})$ or $\tau_V^* \cdot (\hat{z} \times \mathbf{p})$ can be

realized in subspaces $\{|+1\rangle, |0\rangle\}_T$ or $\{|0\rangle, |-1\rangle\}_V$ by applying the Raman coupling between two spin states using a standing-wave and a plane-wave Raman lasers. For the experiment from Ref. [33], different forms of the SO coupling are tuned by adjusting a phase term $\delta\varphi_L$, which is the accumulated relative phase between two Raman beams when both travel through a given optical path. τ_T and τ_T^* terms correspond to $\delta\varphi_L = \frac{\pi}{2}$ and $-\frac{\pi}{2}$, respectively.

In order to generate coherent superposition of two different SO couplings in different subspaces, two plane-wave and one standing-wave Raman lasers are used to couple $\{|+1\rangle, |0\rangle\}_T$ and $\{|0\rangle, |-1\rangle\}_V$, respectively, as illustrated in Fig. 3. Because of different forms of SO couplings τ_T and τ_V^* in different subspaces, we need $\delta\varphi_L = -\frac{\pi}{2}$ for $\{|+1\rangle, |0\rangle\}_T$ and $\frac{\pi}{2}$ for $\{|0\rangle, |-1\rangle\}_V$ using the same optical path. However, the phase tuning is unrealistic here due to the small frequency difference between R_1 and R_3 . We circumvent this issue by choosing the laser frequency configuration in Fig. 3(b). Here the blue plane-wave R_1 and red standing wave R_2 induce the Raman coupling $\sim \Omega_{R_1}\Omega_{R_2}^*$ between $|+1\rangle$ and $|0\rangle$, while the red standing wave R_2 and green plane-wave R_3 induce the coupling $\sim \Omega_{R_2}\Omega_{R_3}^*$ between $|0\rangle$ and $|-1\rangle$. Ω_{R_i} is the Rabi frequency for corresponding Raman laser R_i . When $\Omega_{R_1} = \Omega_{R_3}$, the complex conjugate condition could be satisfied, which realizes the desired STM coupling in Hamiltonian Eq. 4. More details about the experimental scheme and the resulting SO coupling can be found in the supplementary materials [38].

Discussions and Conclusions. There are other types of SO coupling, besides the discussed Rashba-type $\tau \cdot (\hat{z} \times \mathbf{p})$, leading to higher-rank SHE as well. For instance, we mix Dresselhaus and Rashba types in a spin-1 Hamiltonian

$$H_{\text{Mix}} = \frac{p^2}{2m} - \frac{1}{\sqrt{2}} \frac{\lambda}{\hbar} ((\tau_T \cdot (\hat{z} \times \mathbf{p}) + \tau_V \cdot \mathbf{p}), \quad (12)$$

which yields a universal intrinsic rank-2 SHE with $\sigma_{xy}^{zz} = \frac{e}{4\pi}$. In general, the characterization and symmetry requirement of the SO coupling for realizing higher-rank SHEs would be an interesting topic to study.

In conclusion, we introduce and characterize the concept of higher-rank SHE in large spin systems and propose an experimental scheme to realize required STM coupling using cold fermionic atoms. There are many physics remaining to be explored, such as the general construction of rank- n SHE in arbitrary spin systems, quantized higher-rank SHE that will enrich the category of topological insulators [39], the effects of many-body interaction or disorders, extrinsic higher-rank SHE, experimental proposal in solid-state materials with exotic effective pseudospin-1 fermions in 2D [40], etc. Our work defines a new class of SHEs and opens the door for designing large-spin devices with novel functionalities for spintronic applications.

Acknowledgements: We thank Fan Zhang for helpful discussion. This work was supported by Air Force Office of Scientific Research (FA9550-16-1-0387), National Science Foundation (PHY-1806227), and Army Research Office (W911NF-17-1-0128).

-
- [1] J. E. Hirsch, Spin Hall Effect, *Phys. Rev. Lett.* **83**, 1834 (1999).
- [2] J. Sinova, S. O. Valenzuela, J. Wunderlich, C. H. Back, and T. Jungwirth, Spin Hall effects, *Rev. Mod. Phys.* **87**, 1213 (2015).
- [3] T. Seki et al., Giant spin Hall effect in perpendicularly spin-polarized FePt/Au devices, *Nat. Mater.* **7**, 125 (2008).
- [4] L. Liu et al., Spin-Torque Switching with the Giant Spin Hall Effect of Tantalum, *Science* **336**, 555 (2012).
- [5] Y. Niimi et al., Giant Spin Hall Effect Induced by Skew Scattering from Bismuth Impurities inside Thin Film CuBi Alloys, *Phys. Rev. Lett.* **109**, 156602 (2012).
- [6] E. Saitoh, M. Ueda, and H. Miyajima, Conversion of spin current into charge current at room temperature: Inverse spin-Hall effect, *Appl. Phys. Lett.* **88**, 182509 (2006).
- [7] T. Kimura, Y. Otani, T. Sato, S. Takahashi, and S. Maekawa, Room-Temperature Reversible Spin Hall Effect, *Phys. Rev. Lett.* **98**, 156601 (2007).
- [8] B. F. Miao, S. Y. Huang, D. Qu, and C. L. Chien, Inverse Spin Hall Effect in a Ferromagnetic Metal, *Phys. Rev. Lett.* **111**, 066602 (2013).
- [9] J.-C. Rojas-Sánchez et al., Spin Pumping and Inverse Spin Hall Effect in Platinum: The Essential Role of Spin-Memory Loss at Metallic Interfaces, *Phys. Rev. Lett.* **112**, 106602 (2014).
- [10] M. Kimata et al., Magnetic and magnetic inverse spin Hall effects in a non-collinear antiferromagnet, *Nature* **565**, 627(2019).
- [11] C. L. Kane and E. J. Mele, Quantum Spin Hall Effect in Graphene, *Phys. Rev. Lett.* **95**, 226801 (2005).
- [12] B. A. Bernevig, T. L. Hughes, S.-C. Zhang, Quantum Spin Hall Effect and Topological Phase Transition in HgTe Quantum Wells, *Science* **314**, 1757 (2006).
- [13] M. König, S. Wiedmann, C. Brune, A. Roth, H. Buhmann, L. W. Molenkamp, X.-L. Qi, S.-C. Zhang, Quantum Spin Hall Insulator State in HgTe Quantum Wells, *Science* **318**, 766 (2007).
- [14] Y. K. Kato, R. C. Myers, A. C. Gossard, D. D. Awschalom, Observation of the Spin Hall Effect in Semiconductors, *Science* **306**, 1910 (2004).
- [15] S. Murakami, N. Nagaosa, and S. C. Zhang, Dissipationless Quantum Spin Current at Room Temperature, *Science* **301**, 1348 (2003).
- [16] J. Sinova, D. Culcer, Q. Niu, N. A. Sinitsyn, Universal Intrinsic Spin Hall Effect, *Phys. Rev. Lett.* **92**, 126603 (2004).
- [17] Y. Kawaguchi and M. Ueda, Spinor Bose-Einstein condensates, *Phys. Rep.* **520**, 253 (2012).
- [18] B. Bradlyn et al., Beyond Dirac and Weyl fermions: Unconventional quasiparticles in conventional crystals, *Science* **353**, 6299 (2016).
- [19] H. Hu, J. Hou, F. Zhang, and C. Zhang, Topological Triply Degenerate Points Induced by Spin-Tensor Momentum Couplings, *Phys. Rev. Lett.* **120**, 240401 (2018).
- [20] B. Q. Lv et al., Observation of three-component fermions in the topological semimetal molybdenum phosphide, *Nature* **546**, 627 (2017).
- [21] D. L. Campbell, R. M. Price, A. Putra, A. Valdés-Curiel, D. Trypogeorgos & I. B. Spielman, Magnetic phases of spin-1 spin-orbit-coupled Bose gases, *Nat. Commun.* **7**, 10897 (2016).
- [22] X. Luo, L. Wu, J. Chen, Q. Guan, K. Gao, Z.-F. Xu, L. You & R. Wang, Tunable atomic spin-orbit coupling synthesized with a modulating gradient magnetic field, *Sci. Rep.* **6**, 18983 (2016).
- [23] T. Ollikainen, A. Blinova, M. Möttönen, and D. S. Hall, Decay of a Quantum Knot, *Phys. Rev. Lett.* **123**, 163003 (2019).
- [24] K. Sun, C. Qu, Y. Xu, Y. Zhang, and C. Zhang, Interacting spin-orbit-coupled spin-1 Bose-Einstein condensates, *Phys. Rev. A* **93**, 023615 (2016).
- [25] Z.-Q. Yu, Phase transitions and elementary excitations in spin-1 Bose gases with Raman-induced spin-orbit coupling, *Phys. Rev. A* **93**, 033648 (2016).
- [26] G. I. Martone, F. V. Pepe, P. Facchi, S. Pascazio, and S. Stringari, Tricriticalities and Quantum Phases in Spin-Orbit-Coupled Spin-1 Bose Gases, *Phys. Rev. Lett.* **117**, 125301 (2016).
- [27] X.-W. Luo, K. Sun, and C. Zhang, Spin-Tensor-Momentum-Coupled Bose-Einstein Condensates, *Phys. Rev. Lett.* **119**, 193001 (2017).
- [28] E. J. König and J. H. Pixley, Quantum Field Theory of Nematic Transitions in Spin-Orbit-Coupled Spin-1 Polar Bosons, *Phys. Rev. Lett.* **121**, 083402 (2018).
- [29] I. Kuzmenko, T. Kuzmenko, Y. Avishai, and M. Sato, Spin-orbit coupling and topological states in an $F = \frac{2}{3}$ cold Fermi gas, *Phys. Rev. B* **98**, 165139 (2018).
- [30] J. Hou, H. Hu, C. Zhang, Topological phases in spin-1 Fermi gases with two-dimensional spin-orbit coupling, *arXiv:1809.04537* (2018).
- [31] G. Palumbo and N. Goldman, Revealing Tensor Monopoles through Quantum-Metric Measurements, *Phys. Rev. Lett.* **121**, 170401 (2018).
- [32] G. Palumbo and N. Goldman, Tensor Berry connections and their topological invariants, *Phys. Rev. B* **99**, 045154 (2019).
- [33] Z. Wu et al., Realization of two-dimensional spin-orbit coupling for Bose-Einstein condensates, *Science* **354**, 83 (2016).
- [34] Robert N. Cahn, *Semi-Simple Lie Algebras and Their Representations*, Benjamin/Cummings (1984).
- [35] G. Kimura, The Bloch vector for N-level systems, *Phys. Lett. A* **314**, 339 (2003).
- [36] L. H. Huang et al., Experimental realization of two-dimensional synthetic spin-orbit coupling in ultracold Fermi gases, *Nat. Phys.* **12**, 540 (2016).
- [37] Z. Meng et al., Experimental observation of a topological band gap opening in ultracold Fermi gases with two-dimensional spin-orbit coupling, *Phys. Rev. Lett.* **117**, 235304 (2016).
- [38] See supplementary materials for details about SU(2) subalgebras of SU(N) and experimental proposal.
- [39] M. Z. Hasan and C. L. Kane, Colloquium: Topological insulators, *Rev. Mod. Phys.* **82**, 3045 (2010).
- [40] S.-S. Wang et al., Monolayer Mg₂C: Negative Poisson's ratio and unconventional two-dimensional emergent

fermions, [Phys. Rev. Materials](#) **2**, 104003 (2018).

Supplementary Material for “Universal intrinsic higher-rank spin Hall effects”

SU(2) subalgebra of SU(N). We consider a $SU(N)$ Lie group, whose defining representation can be expressed as the generalized Gell-Mann Matrix

$$\begin{aligned}\lambda_{j,k}^S &= I_{j,k} + I_{k,j}, \lambda_{j,k}^A = -i(I_{j,k} - I_{k,j}), \\ \lambda_l^D &= \sqrt{\frac{2}{l(l+1)}} \left(\sum_{m=1}^l I_{m,m} - lI_{l+1,l+1} \right),\end{aligned}\quad (\text{S13})$$

where $1 \leq j < k \leq N$, $1 \leq l \leq N-1$ and $I_{j,k}$ denotes the matrix with a 1 in the (j,k) th entry and 0 elsewhere. We could similarly write down all different $SU(2)$ subalgebras as

$$\tau_{j,k} = \{\lambda_{j,k}^S, \lambda_{j,k}^A, \mathbf{c}_{j,k}^l, \lambda_l^D\}, \quad (\text{S14})$$

where $\mathbf{c}_{j,k}$ is some real vector so that the structure constant of the $SU(2)$ subalgebra is maintained.

Experimental realization. In this section, we discuss the experimental scheme for realizing required STM coupling for rank-2 SHE in a pseudospin-1 fermionic cold gas. Both laser configuration and level diagram are illustrated in Fig. S1 with more details. As 2D SO coupling has been realized in both bosonic and fermionic cold-atom platforms [33, 36], the proposed experimental scheme can be readily implemented with the state-of-art experimental technologies.

In Fig. S1(a), two beams (red) are incident from both x and z directions and reflected by two mirrors to form standing waves $\mathbf{E}_{2x} = \hat{z}E_{2x}e^{i(\varphi_{2x} + \varphi_{2z} + \varphi_L)/2} \cos(k_0x + \alpha)$ and $\mathbf{E}_{2z} = \hat{x}E_{2z}e^{i(\varphi_{2x} + \varphi_{2z} + \varphi_L)/2} \cos(k_0z + \beta)$, where $E_{2x(z)}$ is field strength, $\varphi_{2x(z)}$ is the initial phase, $\varphi_L = k_0K$ is the phase picked up from optical path K and $\alpha(\beta) = (\varphi_{2x(z)} - \varphi_{2z(x)} - \varphi_L)/2$. Another two laser beams (blue and green) are incident in z direction as plane waves $\mathbf{E}_{1(3)z} = \hat{x}E_{1(3)z}e^{i(k_0z + \varphi_{1(3)})}$ and $\mathbf{E}_{1(3)x} = \hat{z}E_{1(3)x}e^{i(-k_0x + \varphi_{1(3)} + \varphi_L - \delta\varphi_{L1(3)})}$ with the initial phases $\varphi_{1(3)}$ and relative phases $\delta\varphi_{L1(3)} = (\omega_2 - \omega_{1(3)})K/c$.

A similar scheme has been studied in our previous work [30], where a low-energy Hamiltonian $k_z F_x + k_x F_y$ has been realized. Such a model describes a rank-1 SHE as we have discussed in the main text. The standing-wave laser will induce a spin-independent lattice potential in this case

$$V(\mathbf{r}) = V_{0x} \cos^2(k_0x + \alpha) + V_{0z} \cos^2(k_0z + \beta), \quad (\text{S15})$$

where $V_{0x(z)}$ are constants. The Raman coupling between $|+1\rangle$ and $|0\rangle$ can be written as

$$M_{1z,2x} = \sum_F \frac{\Omega_{1z,F,9/2}^* \Omega_{2x,F,7/2}}{\Delta_p}, M_{1x,2z} = \sum_F \frac{\Omega_{1x,F,9/2}^* \Omega_{2z,F,7/2}}{\Delta_p}, \quad (\text{S16})$$

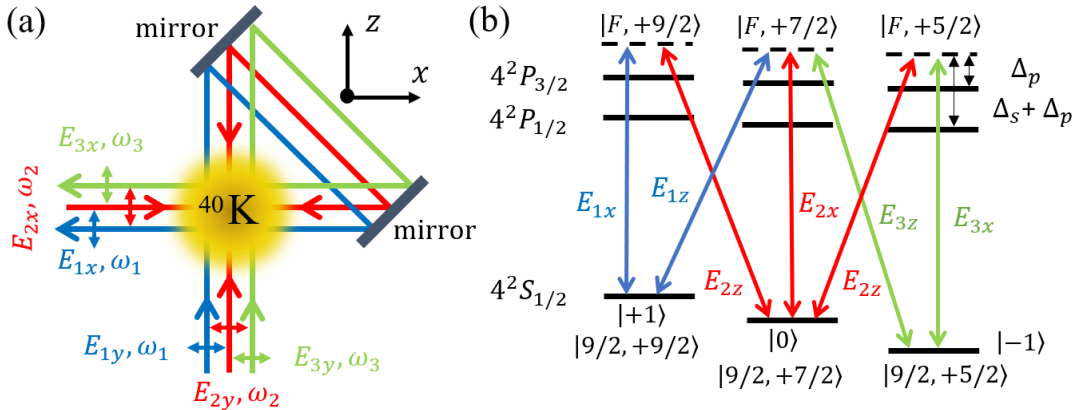


FIG. S1: (a) Experimental scheme for realizing STM coupling of rank-2 SHE in three-component fermionic ^{40}K atomic gases. The desired 2D SO coupling is realized through a standing wave $\mathbf{E}_{2x(z)}$ and two plane-wave $\mathbf{E}_{1(3)x(z)}$ laser fields. The arrows indicate the incident directions of the laser beams and each beam is reflected by two mirrors. (b) Level diagram and optical coupling in the hyperfine structure $|F, m\rangle$ of ^{40}K atoms. F is the quantum number of hyperfine states and Δ_s denotes fine-structure splitting.

where the effective Rabi frequency is

$$\Omega_{ix,F,m_\sigma} = e\langle \frac{9}{2}, m_\sigma | z | F, m_\sigma \rangle \hat{z} \cdot \mathbf{E}_{ix}, i = 1, 2 \quad (\text{S17})$$

$$\Omega_{1z,F,m_\sigma} = e\langle \frac{9}{2}, m_\sigma | x | F, m_\sigma + 1 \rangle \hat{x} \cdot \mathbf{E}_{1z}, \quad \Omega_{2z,F,m_\sigma} = \langle \frac{9}{2}, m_\sigma | x | F, m_\sigma - 1 \rangle \hat{x} \cdot \mathbf{E}_{2z}$$

and we have neglected the transitions to $D1$ line due to larger fine-structure splitting $\Delta_s \approx 2\pi \times 1.7\text{THz} \gg \Delta_p$. After expanding the effective Rabi frequency, we obtain

$$M_{1z,2x} = M_{0x} \cos(k_0x + \alpha) e^{-i(k_0z + \beta)} e^{i(\varphi_{2z} - \varphi_1)}, \quad (\text{S18})$$

$$M_{1x,2z} = M_{0y} \cos(k_0z + \beta) e^{i(k_0x + \alpha)} e^{i(\varphi_{2z} - \varphi_1 + \delta\varphi_{L1})}, \quad (\text{S19})$$

and $M_{0x(y)}$ are coupling constants that can be tuned through individual laser intensity. Similarly, the Raman coupling between $|0\rangle$ and $|-1\rangle$ can be written as

$$M_{2z,3x} = \sum_F \frac{\Omega_{2x,F,7/2}^* \Omega_{3z,F,5/2}}{\Delta_p} = M'_{0x} \cos(k_0x + \alpha) e^{i(k_0z + \beta)} e^{i(-\varphi_{2z} + \varphi_3)} \quad (\text{S20})$$

$$M_{2x,3z} = \sum_F \frac{\Omega_{2z,F,7/2}^* \Omega_{3x,F,5/2}}{\Delta_p} = M'_{0y} \cos(k_0z + \beta) e^{-i(k_0x + \alpha)} e^{i(-\varphi_{2z} + \varphi_3 - \delta\varphi_{L3})}. \quad (\text{S21})$$

We note that terms proportional to $\cos(k_0x + \alpha) \cos(k_0z + \beta)$ are antisymmetric to each lattice site in both x and y directions and thus can be neglected for low-band physics. The Raman coupling terms are further simplified as

$$\mathcal{M}_{+1,0} = (M_x - M_y \cos \delta\varphi_{L1}) - iM_y \sin \delta\varphi_{L1}, \quad (\text{S22})$$

$$\mathcal{M}_{0,-1} = (M'_x - M'_y \cos \delta\varphi_{L3}) + iM'_y \sin \delta\varphi_{L3}, \quad (\text{S23})$$

where $M_x = M_{0x} \cos(k_0x + \alpha) \sin(k_0z + \beta)$, $M_y = M_{0y} \cos(k_0z + \beta) \sin(k_0x + \alpha)$ and $M'_{x(y)}$ are defined similarly. In the above equations, we also choose the initial phase of the lasers so that $e^{i(\varphi_{2z} - \varphi_1)} = i$ and $e^{i(-\varphi_{2z} + \varphi_3)} = -i$. Since $|\omega_1 - \omega_3|/\omega_2 \ll 1$, we have $\delta\varphi_{L1} \approx \delta\varphi_{L3} = \delta\varphi_L$. Assuming the coupling constants are tuned to be equivalent $M'_x = M_x$ and $M'_y = M_y$, the total effective Hamiltonian becomes

$$H = \frac{\mathbf{p}^2}{2m} + V(\mathbf{r}) + \mathcal{M}_x(\lambda_1 + \lambda_6) + \mathcal{M}_y(\lambda_2 - \lambda_7) + \frac{\delta_T}{2} F_z^2 + \frac{\delta_V}{2} F_z, \quad (\text{S24})$$

where $\mathcal{M}_x = M_x - M_y \cos \delta\varphi_L$, $\mathcal{M}_y = M_y \sin \delta\varphi_L$ and the Zeeman terms are incorporated into the detunings in the ground-state manifold. When $\delta\varphi_L = \pi/2$, the SO coupling becomes $M_x(\lambda_1 + \lambda_6) + M_y(\lambda_2 - \lambda_7)$.

As we consider the lowest s -orbital $\phi_{s,\sigma}$ ($\sigma = +1, 0, -1$) and nearest-neighbor hopping, the SO coupling part of the tight-binding Hamiltonian can be written as

$$H_{\text{SOC}} = \sum_{\langle i,j \rangle} \left(t_{\text{so},+}^{ij} \hat{c}_{i+1}^\dagger \hat{c}_{j,0} + h.c. + t_{\text{so},-}^{ij} \hat{c}_{i,0}^\dagger \hat{c}_{j,-1} + h.c. \right), \quad (\text{S25})$$

where hopping strengths can be expressed as overlap integrals

$$t_{\text{so},+}^{ij} = \int d^2\mathbf{r} \phi_{s,+1}^i(\mathbf{r}) [M_x(x,y)(\lambda_1 + \lambda_6) + M_y(x,y)(\lambda_2 - \lambda_7)] \phi_{s,0}^j(\mathbf{r}), \quad (\text{S26})$$

$$t_{\text{so},-}^{ij} = \int d^2\mathbf{r} \phi_{s,0}^i(\mathbf{r}) [M_x(x,y)(\lambda_1 + \lambda_6) + M_y(x,y)(\lambda_2 - \lambda_7)] \phi_{s,-1}^j(\mathbf{r}). \quad (\text{S27})$$

Finally, the SO coupling in low-energy Bloch Hamiltonian reads $\lambda_{\text{SO}} k_x (\lambda_1 + \lambda_6) + \lambda_{\text{SO}} k_z (\lambda_2 - \lambda_7)$, $\lambda_{\text{SO}} = 2t_{\text{SO}}$, which realizes the desired STM coupling for rank-2 SHE discussed in Equ. 4.